Detection of prompt-γ with BaF_2 crystal emitted by 220 MeV/u ^{12}C ion interaction with PMMA

M. Vanstalle[a], **F. Bellini**[b,c], **F. Bini**[d], **F. Collamati**[b,c], **E. De Lucia**[e], **M. Durante**[f], **R. Faccini**[b,c], **F. Ferroni**[b,c], **Ch. Finck**[a], **S. Fiore**[g], **P. Gauzzi**[b,c], **E. Iarocci**[e,h], **M. Marafini**[b,i], **I. Mattei**[e,j], **V. Patera**[e,h], **L. Piersanti**[e,h], **A. Sarti**[e,h], **C. Schuy**[f], **A. Sciubba**[e,h], **C. Voena**[b,c], **C. La Tessa**[k]

[a] IPHC, Strasbourg, France
[b] Dipartimento di Fisica, Sapienza Università di Roma, Roma, Italy
[c] INFN Sezione di Roma, Roma, Italy
[d] Dipartimento di Ingegneria Meccanica e Aerospaziale, Sapienza Università di Roma, Roma, Italy
[e] Laboratori Nazionali di Frascati dell'INFN, Frascati, Italy
[f] GSI, Darmstadt, Germany
[g] ENEA
[h] Dipartimento di Scienze di Base e Applicate per Ingegneria, Sapienza Università di Roma, Roma, Italy
[i] Museo Storico della Fisica e Centro Studi e Ricerche "E. Fermi", Roma, Italy
[j] Dipartimento di Matematica e Fisica, Roma Tre Università di Roma, Roma, Italy
[k] Brookhaven National Laboratory, Uptown NY, USA

Abstract. The real time monitoring of the Spread-Out-Bragg-Peak (SOBP) position poses one of the major challenges in modern ion therapy as it would allow a direct verification of the patient alignment in combination with the treatment planning delivered. A possible method to achieve this goal is to exploit the emission of secondary particles by nuclear interactions of the primary ions with the patient and correlate their trajectory and yield to the tumor position.
In this study, we measured the prompt-γ spectra as well as the production rate of these photons, produced by nuclear interactions of a 220 MeV/u ^{12}C beam with a PMMA target. The data were compared to Monte Carlo simulations performed with Geant4. A good qualitative agreement was obtained between energy spectra (experimental and simulated), as a good agreement between overall experimental and simulated prompt-γ yields. The results presented in this work also indicate that QMD and INCL models are more suitable for simulating prompt-γ originating from ^{12}C interaction than BIC model.
At last, we conclude that the clinical application of the prompt-γ monitoring will suffer from low statistics, which implies a limited resolution on the SOBP monitoring.

PACS numbers:

Introduction

The determination of the irradiated volume position is a major concern in modern ion therapy as it provides a check of the maximal dose deposited in the tumor and in the peripheral healthy tissue. At the moment, this clinical dose control is performed with the Positron Emission Tomography (PET) technique, which works in an offline mode. A real time dose control of the irradiated volume position would allow an online monitoring of the patient alignment in combination with the treatment planning delivered [1]. This aspect is of key importance for therapy with carbon ion beams, where the dose profile is very sensitive to anatomical changes and minor patients repositioning uncertainties. Most methods to achieve this goal are based on exploiting the fragmentation of the primary ions in the patient, correlating the production of secondary particles with the treatment planning. The approaches considered so far are based on tracking secondary protons [2, 3, 4], detecting prompt-γ [5, 6] or by online PET monitoring [7, 8, 9]. One important parameter in these methods is the yield of secondaries produced during the treatment, from which the Bragg peak position resolution is directly dependent.
This work presents the characterization of prompt-γ produced by nuclear interactions of 220 MeV/u carbon ions in a PMMA target. The measurements include yield and energy spectra of photons emitted at 60° and 90° with respect to the primary beam direction. All results are compared with predictions from Geant4 Monte Carlo code.

1. Experimental setup

The experiment was performed at the experimental cave A in GSI, Darmstadt, Germany. The experimental setup was similar to the one described in [10] and is presented on Fig.1. The 220 MeV/u fully stripped ^{12}C beam impinged a 5×5×20 cm^3 PMMA target, thick enough to completely stop the primary ions. The beam spot was Gaussian shaped, with standard deviation in the transverse plane $\sigma_{\text{beam}} \simeq 1$ cm, measured with 1% relative uncertainty by the GSI beam monitor chambers. The beam intensity was monitored by two 1.1 mm thick plastic scintillators (referred to as SC1 and SC2 respectively) placed at 16 and 37 cm upstream of the PMMA target, respectively. Each scintillator was coupled with two photomultiplier tubes (PMTs: Hamamatsu 10580) on each side. The start counters time and charge information were both acquired, but only scintillator closest to the target (SC2) was used to build the trigger signal (OR of the two PMTs). All detectors downstream of the target were mounted on arms which could be rotate at several angles from the primary beam direction to acquire data at different angular positions. On each side of the target the produced fragments were characterized with a ΔE-E telescope composed of a plastic scintillator and a crystal (LYSO or barium fluoride BaF_2). In this paper, we will focus only on data acquired with the BaF_2 detector as the other results are discussed elsewhere [?].

The BaF_2 scintillator, similar as the one described in [11], was placed at 73 cm from the target center and acquired the residual energy of charged and uncharged secondary

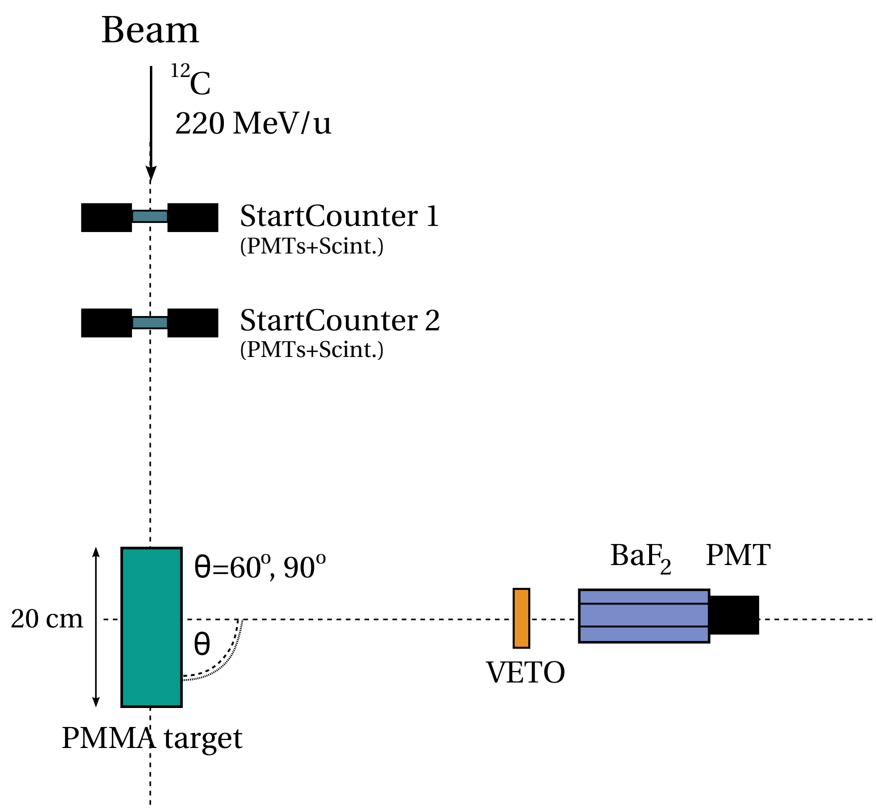

Figure 1. Scheme of the experimental setup.

particles. It is hexagonally-shaped with a circumscribe radius of 5.4 cm and a length of 14 cm (crystal part only), and surrounded by a 1 mm thick aluminum layer. More details on the crystal properties can be found in [12]. The scintillation light of the crystal was collected by a PMT. A $10\times10\times0.2$ cm^3 plastic scintillator, referred to as VETO, was placed in front of the BaF crystal for measuring the energy loss ΔE of charged particles and discriminate them from neutral radiation.

The trigger signal for the data acquisition system was provided by the coincidence within 80 ns time window between the signal of the SC2 and the signals of the BaF_2 and LYSO detector. The threshold to discriminate the signal from the BaF_2 PMT was set to 200 mV, and the high voltage applied was 2000 V.

The front-end electronics was read-out by a VME system. The time signal of all the detectors was acquired by a 19-bit TDC Multi-hit with a resolution of 100 ps, while the collected charge was measured with a 12-bit QDC. The number of incident carbon ions impinging on the target (referred to as N_C) are measured with a scaler, counting the number of AND signals built from the output of SC2 PMTs.

Particle identification was achieved using the correlation between the residual energy information (E) and Time-of-Flight (ToF) measurement between the start counters and the crystal.

2. Calibration of the barium fluoride

In order to calibrate the charge acquired by the detector in kinetic energy, the barium fluoride was irradiated with four γ sources : ^{22}Na (0.511 and 1.275 MeV), ^{137}Cs (0.662 MeV), ^{60}Co (1.17 and 1.33 MeV) and ^{239}PuBe (peak at 4.431 MeV from $^{12}C^*$ decay). The resulting calibration curve is linear in the energy range of interest for this work (1-10 MeV). The average energy resolution is around 8% and is deteriorated by the presence of an internal source, coming from α-emitters impurities (^{226}Ra, ^{222}Rn, ^{218}Po, ^{214}Po).

3. Prompt-γ selections

The energy deposition in the crystal (E) is combined with the time of flight (ToF) spectrum to separate mainly prompt-γ from neutrons and residual of other secondary charged fragments. The ToF is computed as the time difference between the signal detected in the SC induced by the carbon ion and the signal from the BaF_2. Note that the ToF is not the real time of flight, because the time difference between a carbon ion interacting in the SC2 and its prompt-γ emission in the PMMA ($\simeq$2 ns) was not taken into account.
The slowing-down effect induced by the front-end electronics fixed voltage threshold has been considered [13]. The energy deposited in the crystals is obtained by converting the QDC-channels in MeV using the calibration presented is the previous section. The analysis of the two dimensional space plots (E,ToF), shown in Fig.2, provides a highly efficient selection of a pure sample of prompt photons. Two horizontal bands appear in the low energy region: the lower one is due to electronic noise, while the higher band is generated by random coincidences with the internal α-source. The vertical band centered at 0 ns corresponds to the γ signal of interest, while the events with a ToF higher than 0 correspond to neutrons, considered as physical noise.

4. Monte Carlo validation

Monte Carlo simulations of the experiment have been carried out with Geant4 [14], using three different models: the QMD model of ion-ion collisions, described in [15], the Binary Cascade light ion model (BIC), described in [16], and the Lige intra-nuclear cascade model INCL++ described in [17]. These models were chosen for their better agreement with the experimental data [18, 19]. Each model is validated by comparing its predictions with the experimental *raw* γ spectra, i.e. without applying any corrections for detector and geometrical efficiency. However, these spectra have been normalized by the number of incident carbon ions N_C and by the dead time τ.
To produce the experimental spectra, we need to compute the number of prompt-γ N_γ. To obtain this quantity, the 2D (E,ToF) distribution is divided into 0.1 MeV energy slices, chosen in agreement with the energy resolution of the detector at 1 MeV. Then

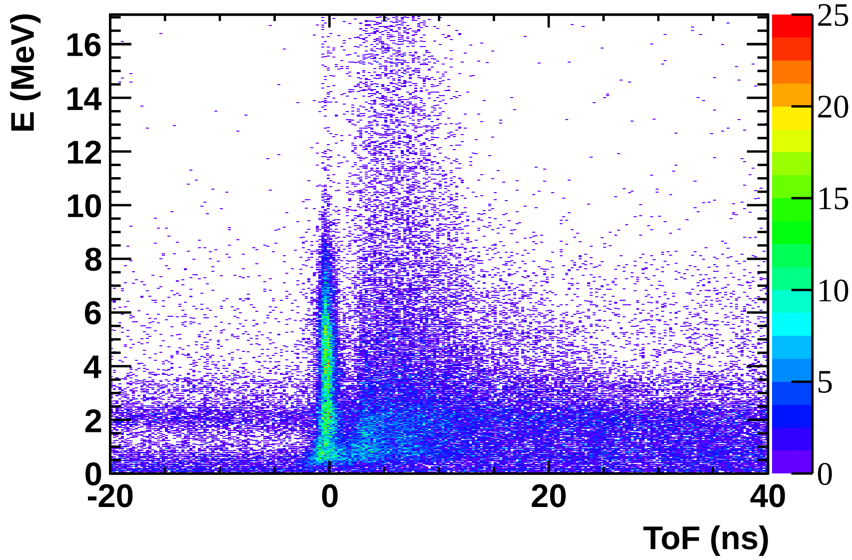

Figure 2. (color online) Energy deposition in the BaF_2 crystal as a function of ToF.

the number of prompt-γ in each energy bin is extracted using an unbinned maximum likelihood fit, thanks to the RooFit package from ROOT [20]. The background, mainly due to neutrons, is described by a polynomial function convoluted with a Landau distribution while the signal is modeled using a Gaussian function. The number of prompt photons is hence extracted from the extended likelihood fit, to the ToF distribution for each energy slice.

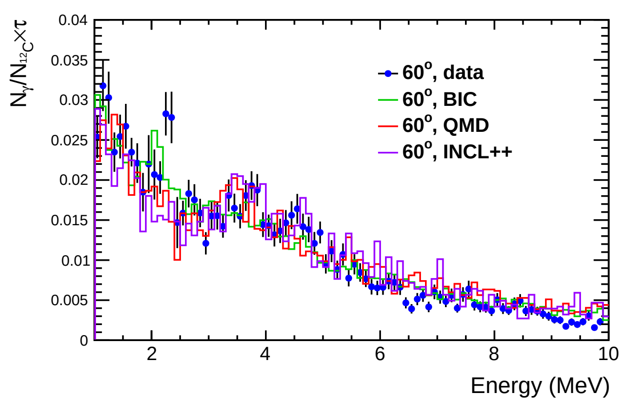

Figure 3. Normalized energy spectra of prompt-γ detected by the barium fluoride at 60°. Predictions from QMD, INCL and BIC models are shown too.

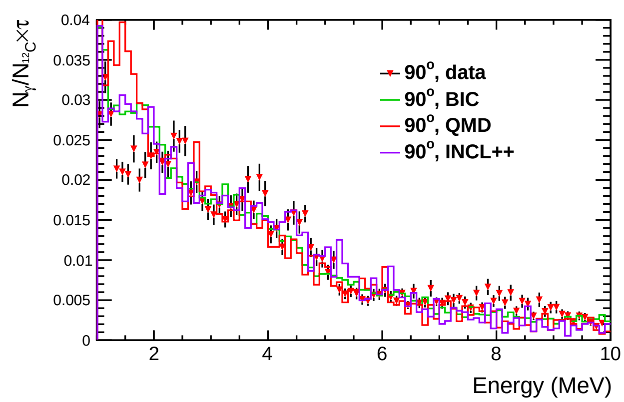

Figure 4. Normalized energy spectra of prompt-γ detected by the barium fluoride at 90°. Predictions from QMD, INCL and BIC models are shown too.

The resulting measured energy distributions are shown in Figs. 3 and 4, for 60° and for 90°. On each figure are superimposed the three simulated spectra (QMD, INCL

and BIC). For a better comparison, the presented spectra have been normalized by the number of entries. As previously observed, the agreement between nuclear reaction models used in GEANT4 and the experimental data is not yet optimal [18]. However it can be noticed on both Fig.3 and Fig.4, simulated distributions and experimental one are in good agreement, except for energies below 2 MeV. In this case, the discrepancies between the two distributions originate from the physical noise, coming from neutrons and the internal source of the detector.
The agreement between the simulated and experimental distributions can be quantified using the least-square method. The χ^2/ndf values calculated for energies above 2 MeV are reported in Tab.1: the closest the χ^2/ndf is to 1, the better is the similarity between the compared distributions. These values illustrate the relative good agreement between the shape of the distributions. Nevertheless, we noticed that the discrepancies between Monte Carlo and data are more pronounced in the case of the BIC model. The reduced χ^2 values show that INCL has the better agreement with the data, which can also be seen on the spectra where the 4.4 MeV peak from ^{12}C is well reproduced. The number of detected γ is in relatively good agreement with the data for both QMD and INCL, with a difference by a factor 0.9 with the experiment. Based on these results, INCL model was selected for calculating detection efficiency correction factors.

Angle	χ^2/ndf (BIC)	χ^2/ndf (QMD)	χ^2/ndf (INCL)
60°	7.5	3.8	1.6
90°	11.1	6.6	2.9

Table 1. Reduced χ^2 between experimental and simulated photon yield at 60° and 90°. The values are calculated for energy bins above 2 MeV.

5. Prompt-γ energy spectra

5.1. Correction factors

The prompt-γ yield Φ_γ is calculated from the experimental spectra according to the following equation 1:

$$\Phi_\gamma = \frac{N_\gamma}{N_C \times \tau \times \varepsilon_{det} \times \varepsilon_{geo} \times \Omega} \tag{1}$$

The number of incident carbon ions N_C is measured with the scaler, as already mentioned in the first section. The dead-time τ ranges from few % to 20% depending on the dataset.
The detector efficiency $\varepsilon_{\rm det}$ is defined as the ratio between the number of photons detected and impinging on the detector. This fraction has been calculated for each energy bin of the spectra separately using GEANT4 simulations (INCL model, see Sec.4). The geometrical efficiency $\varepsilon_{\rm geo}$ was also calculated using Monte Carlo simulations, as the γ impinging on the detector divided by the total number of γ emitted from the

target. As the γ source is an extended source (corresponding to the target volume), the efficiency changes with the energy, in such a way that its value has to be calculated for each energy bin (between 1 and 10 MeV) independently. The prompt-γ are not isotropically emitted in the laboratory due to the center of mass velocity. They are preferentially emitted either in the forward direction if they originate from the projectile decay, or isotropically if created by a target nucleus decay. Therefore this phenomenon has to be taken into account into ε_{geo} calculation. In this goal, the anisotropy of the source was simulated with the three GEANT4 models, illustrated by Fig.5. BIC model reproduces poorly the anisotropy of the γ emission, while INCL and QMD are both in agreement. Consequently, the angular distribution generated with QMD (or INCL) was implemented in the calculation of ε_{geo}. It has to be pointed out that the angular distribution used was the same for each simulated γ energy, which is an approximation as some γ are mainly emitted by the target, and consequently are isotropically distributed (i.e. the 4.4 MeV γ-ray from the ^{12}C). The calculated ε_{geo} values are, as expected because of anisotropy, higher for 60° than for 90°, with a constant difference in energy between the two angles.

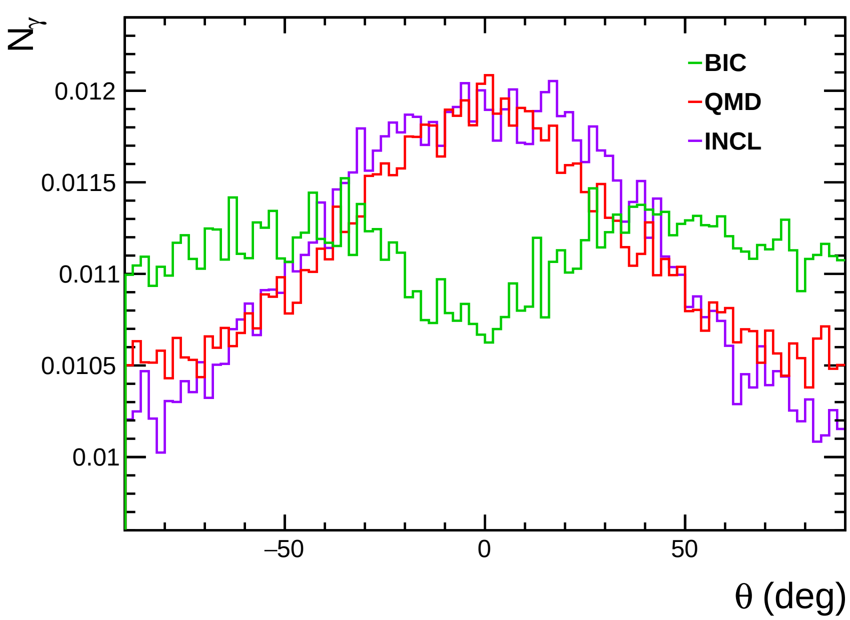

Figure 5. Angular distribution of prompt-γ emitted by interaction of ^{12}C with PMMA target, simulated by GEANT4 (BIC, QMD and INCL).

5.2. Energy spectra

The resulting fully corrected energy spectra are shown on Fig.6. Several peaks are visible in the spectra and originate mainly from the deexcitation of ^{12}C and ^{16}O levels. The main peak located at $\sim$ 4.44 MeV corresponds to the 2^+ level decay, while the bump seen between 3 and 4 MeV is a combination of γ emitted by ^{16}O (2^- at 2.74 MeV) and by ^{12}C ($0_2^+ \rightarrow 2^+$ at 3.21 MeV). The peak located around 6 MeV corresponds to the $0_2^+ \rightarrow 0^+$ (6.05 MeV) and $3^- \rightarrow 0^+$ (6.13 MeV) levels of ^{16}O, while the γ-ray located close to 7 MeV comes from the decay of the $2^+ \rightarrow 0^+$ (6.92 MeV) and the $1^- \rightarrow 0^+$ (7.11 MeV) [21]. The small bump visible around 5 MeV originates from the $5/2^+ \rightarrow 1/2^-$ (5.27 MeV) and $1/2^+ \rightarrow 1/2^-$ (5.29 MeV) decay of the ^{15}N, both produced by inelastic scattering of neutrons with ^{16}O.

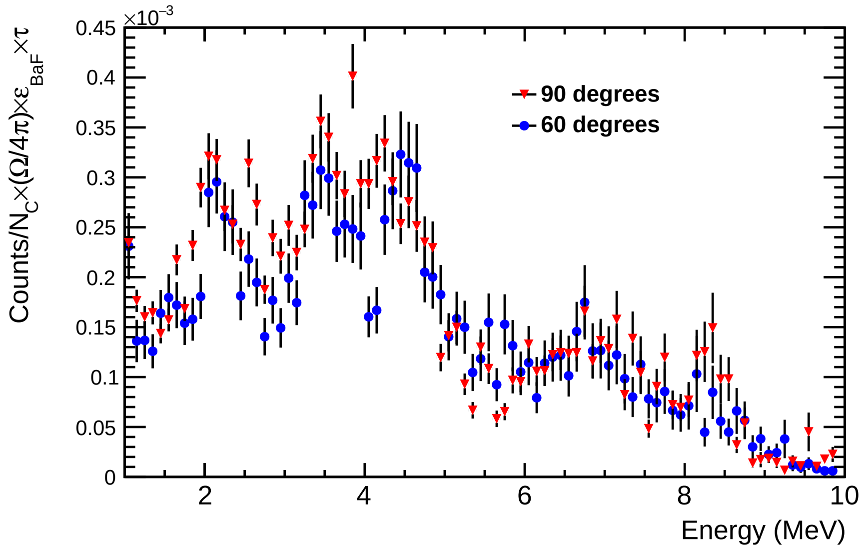

Figure 6. Fully corrected simulated and experimental energy spectra for each measured angle.

5.3. Prompt-γ yield

The final goal of monitoring with prompt-γ is to correlate the production of prompt-γ with the dose delivered to the patient per number of incident carbon ions. An estimation of the prompt-γ flux is required to calculate the total delivered dose[13] and is obtained integrating the energy spectrum between 2 and 10 MeV (see Eq.1). The resulting yields Φ_γ measured with the BaF_2 crystal for each measured angle are presented in Tab.2, together with the simulated values estimated with Geant4 (BIC, QMD and INCL models).

The uncertainties on the experimental values include statistic and systematic contributions. The systematic error is originating from the uncertainty on the dead time τ and on the choice of the Geant4 model for the correction factors calcultation. These factors were determined for each tested models (INCL, BIC and QMD), and the corresponding γ rate was calculated. The standard deviation between the three obtained values corresponds to the systematic uncertainty.

As expected after applying all geometrical and detection correction factors, the total fluxes are the same order of magnitude for both angle, within the error bars. The difference between the two yield values originates from the approximation made in the

anisotropy calculation of the prompt-γ emission (see Sec.5.1), considering a single angular distribution for the overall energy range. This leads to an error on the $\varepsilon_{\rm geo}$ determination.
As a conclusion, the experimental γ yield at 90° for 220 MeV/u ^{12}C beam is 5 times higher than the one measured with 80 MeV/u ^{12}C beam [13]. The GEANT4 simulation of the two experiments confirm this result, predicting a factor 4.9 between the photon emission yield at 80 MeV/u and 220 MeV/u.
Table 2 shows also simulated γ-yield values for comparison with the data. INCL gives the value closest to the data ($\sim$ 10% of difference) and within the error bars, while QMD and BIC overestimates the yield by almost 50% at 60°.

	60°	90°
Data	$(1.15 \pm 0.11)\times10^{-2}$	$(1.29 \pm 0.22)\times10^{-2}$
BIC	$(2.15 \pm 0.02)\times10^{-2}$	$(1.83 \pm 0.02)\times10^{-2}$
QMD	$(2.33 \pm 0.03)\times10^{-2}$	$(1.88 \pm 0.03)\times10^{-2}$
INCL	$(1.31 \pm 0.02)\times10^{-2}$	$(1.09 \pm 0.02)\times10^{-2}$

Table 2. Experimental and simulated (GEANT4 using BIC, QMD and INCL reaction models) differential rates of prompt-γ for each measured angle. The results are presented in $sr^{-1}/^{12}C$.

5.4. Ion inelastic scattering

The comparison between experimental data and Geant4 simulations is illustrated in Fig.7, where the fully corrected energy spectra are plotted for 60°. The agreement is again better for QMD and INCL models, especially for energies higher than 3 MeV, for which BIC model underestimates prompt-γ rates. The 4.44 MeV peak is particularly not well reproduced by BIC, which originates from an underestimation of inelastic scattering processes.
This is shown on Fig.8, where the γ spectra emitted only by (^{12}C+^{12}C) and (^{12}C+^{16}O) inelastic scattering are plotted. Clearly BIC model does not reproduce correctly the γ peaks seen on Fig.7. This is not the case for QMD and INCL, which predict all expected peaks, especially the 3.21 MeV and the 4.44 MeV of the ^{12}C. With INCL and QMD, we also see the 3.21 MeV peak of the ^{12}C and the 2.74 MeV peak of the ^{16}O, and the combination of the 5.27 MeV and 5.29 MeV peaks of the ^{15}N produced in this reaction. These last peaks are presented in details on Fig.9, for all models.

5.5. Neutron inelastic scattering

BIC model also has problems to reproduce correctly the emitted γ spectra for neutron inelastic scattering processes ^{12}C(n,n′) and ^{16}O(n,n′), as illustrated in Fig.10 and 11. For

^{12}C(n,n′) process, BIC is in agreement with QMD and INCL only for the 2^+ decay of ^{12}C, as shown on Fig.10. The other γ peaks present in the spectrum are not corresponding to any identified ^{12}C levels. On the other side, QMD and INCL spectra show the main γ levels of the ^{12}C, including the 0_2^+ (3.21 MeV), the 2^+ and the 3^- (9.64 MeV). BIC limitation is more visible with ^{16}O(n,n′), for which the model does not reproduce any of the expected ^{16}O γ rays, except the 4.44 MeV peak coming from the α decay of ^{16}O into ^{12}C (Fig.11). γ spectra obtained with QMD and INCL show the 2^- level at 2.7 MeV, the 0^+ and 3^- (6.05 and 6.13 MeV), the 2^+ at 6.92 MeV and the 1^- at 7.11 MeV, as expected [21]. The three same γ peaks as in the ^{12}C(n,n′) spectrum, also originated from the α decay of ^{16}O, are also recognizable.
As a consequence, this study indicates that QMD and INCL models are more suitable than BIC for simulating prompt-γ spectra produced by ^{12}C nuclear interaction with PMMA target.

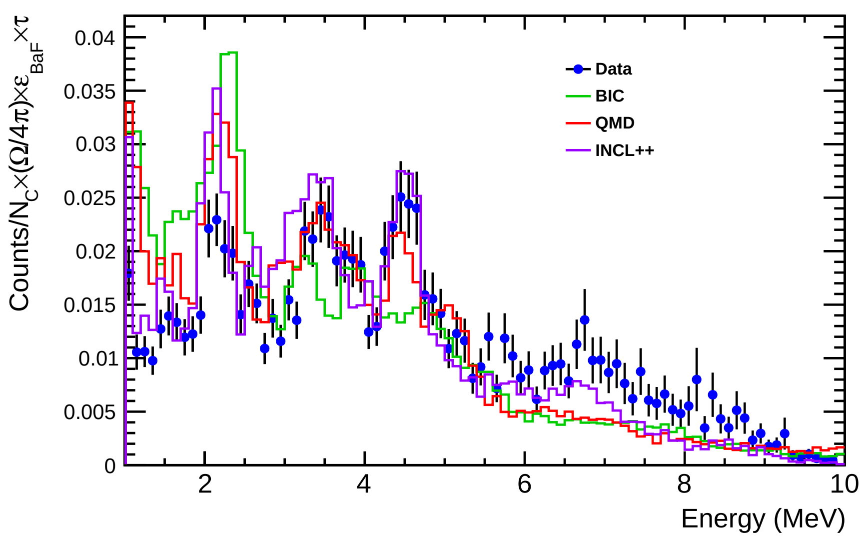

Figure 7. Comparison between experimental and simulated (BIC, INCL and QMD reaction models) corrected energy distributions at 60°. Spectra have been normalized by the number of entries for better comparison.

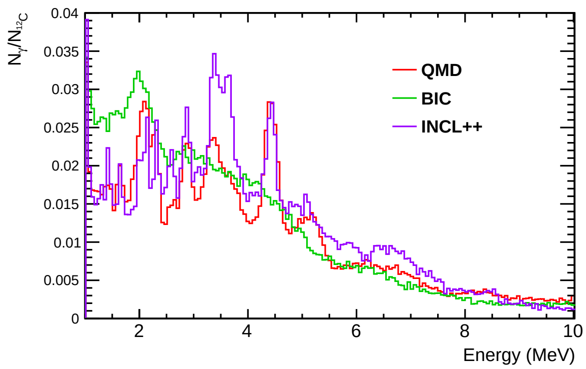

Figure 8. Comparison between BIC, INCL and QMD emitted γ spectra for inelastic scattering between ions (^{12}C+^{12}C) and (^{12}C+^{16}O).

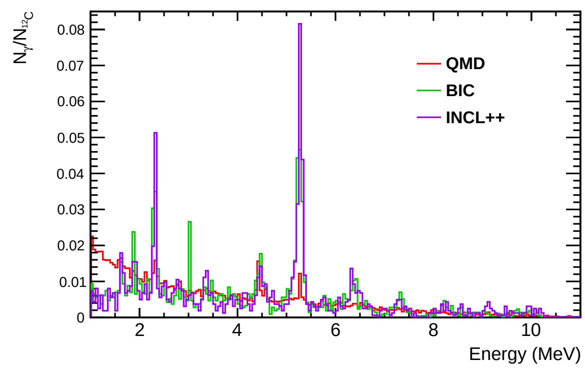

Figure 9. Comparison between BIC, INCL and QMD emitted γ spectra from ^{14}N and ^{15}N decay.

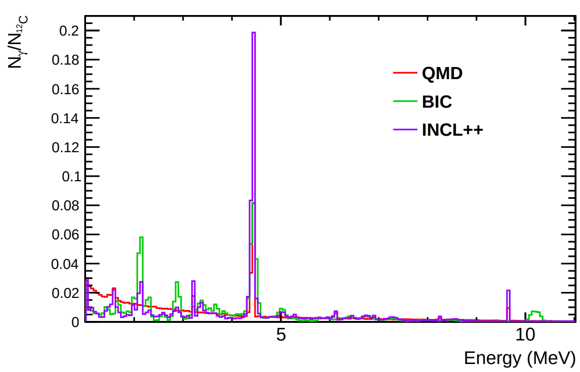

Figure 10. Comparison between BIC, INCL and QMD emitted γ spectra for neutron inelastic scattering ^{12}C(n,n′).

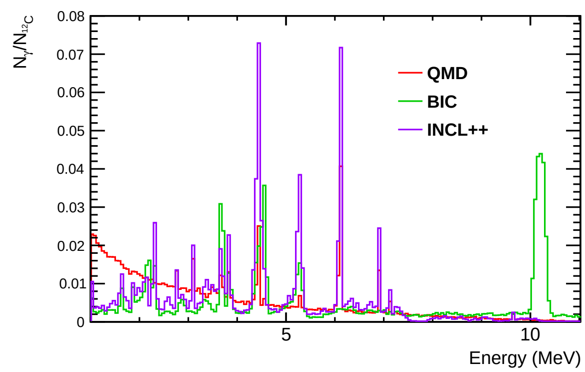

Figure 11. Comparison between BIC, INCL and QMD emitted γ spectra for neutron inelastic scattering ^{16}O(n,n′).

Conclusion

Yields and energy spectra of prompt-γ produced by the interaction of 220 MeV/u carbon ions with PMMA target have been measured at two angles (60° and 90 °) with respect to the primary beam. After applying all corrections, the yield values appear to be in fair agreement:

$$\Phi_\gamma(E > 2MeV, \theta = 90°) = (1.27 \pm 0.02_{\mathrm{stat}} \pm 0.20_{\mathrm{sys}}) \times 10^{-2} sr^{-1} \quad (2)$$

$$\Phi_\gamma(E > 2MeV, \theta = 60°) = (1.10 \pm 0.02_{\mathrm{stat}} \pm 0.09_{\mathrm{sys}}) \times 10^{-2} sr^{-1} \quad (3)$$

The experimental data have been compared to predictions from Geant4 with three different reaction models (BIC, QMD and INCL) to assess their accuracy. The study confirmed that Geant4 models can reproduce well the shape of the prompt-γ spectra

within acceptable agreement. Furthermore, INCL model is more accurate than BIC and QMD to reproduce the γ-yields, as it is the case for charged particles [18, 22]. The discrepancies between BIC and the data originate from the fact that the model does not take into account properly inelastic scattering processes between ions (^{12}C+^{12}C) and (^{12}C+^{16}O), and neutrons scattering.
Yield measurements are crucial in the context of real time monitoring of the SOBP to estimate the feasibility of the method in the clinical context. If we suppose we need $\sim 10^8$ ^{12}C ions to deposit 1 Gy [23], according to our results $\sim 10^6$ prompt-γ will be emitted in the whole environment. The online dose control technique will be limited by the geometrical acceptance of the chosen detector, in such a way that the number of detected prompt-γ will be quite lower and the resolution on the SOBP position will be deteriorated. Consequently, the clinical application will suffer from the low production rate of the γ.

References

[1] A.-C. Knopf and A. Lomax. "In vivo proton range verification: a review". In: *Physics in Medicine and Biology* 58.15 (2013), R131.

[2] K. Gwosch et al. "Non-invasive monitoring of therapeutic carbon ion beams in a homogeneous phantom by tracking of secondary ions". In: *Physics in Medicine and Biology* 58.11 (2013), p. 3755.

[3] P. Henriquet et al. "Interaction vertex imaging (IVI) for carbon ion therapy monitoring: a feasibility study". In: *Physics in Medicine and Biology* 57.14 (2012), p. 4655.

[4] L. Piersanti et al. "Measurement of charged particle yields from PMMA irradiated by a 220 MeV/u ^{12} C beam". In: *Physics in Medicine and Biology* 59.7 (2014), p. 1857.

[5] C.-H. Min et al. "Prompt gamma measurements for locating the dose falloff region in the proton therapy". In: *Applied Physics Letters* 89.18 (2006).

[6] M. Testa et al. "Real-time monitoring of the Bragg-peak position in ion therapy by means of single photon detection". English. In: *Radiation and Environmental Biophysics* 49.3 (2010), pp. 337–343.

[7] J. Pawelke et al. "In-beam PET imaging for the control of heavy-ion tumour therapy". In: *Nuclear Science Symposium, 1996. Conference Record., 1996 IEEE.* Vol. 2. 1996, 1099–1103 vol.2.

[8] K. Parodi, W Enghardt, and T Haberer. "In-beam PET measurements of β^+ radioactivity induced by proton beams". In: *Physics in Medicine and Biology* 47.1 (2002), p. 21.

[9] W. Enghardt et al. "Charged hadron tumour therapy monitoring by means of PET". In: *Nuclear Instruments and Methods in Physics Research Section A: Accelerators, Spectrometers, Detectors and Associated Equipment* 525.12 (2004). Proceedings of the International Conference on Imaging Techniques in Subatomic Physics, Astrophysics, Medicine, Biology and Industry, pp. 284 –288.

[10] K. Gunzert-Marx et al. "Secondary beam fragments produced by 200 MeV/u ^{12}C ions in water and their dose contributions in carbon ion radiotherapy". In: *New Journal of Physics* 10 (2008).

[11] R. Novotny. "The BaF_2 photon spectrometer TAPS". In: *Nuclear Science, IEEE Transactions on* 38.2 (Apr. 1991), pp. 379–385.

[12] S. V. Vladimirov et al. "Characteristics of BaF_2 Scintillation Crystals". In: *Atomic Energy* 90.1 (2001), pp. 55–62.

[13] C. Agodi et al. "Precise measurement of prompt photon emission from 80 MeV/u carbon ion beam irradiation". In: *Journal of Instrumentation* 7 (2012), p03001.

[14] The GEANT4 collaboration. URL: http://geant4.cern.ch.

[15] T. Koi. "New native QMD code in Geant4". In: *IEEE Nuclear Science Symposium Conf. Record* (2008).

[16] G. Folger, V.N. Ivanchenko, and J.P. Wellisch. "The Binary Cascade: nucleon nuclear reactions". English. In: *The European Physical Journal A - Hadrons and Nuclei* 21.3 (2004), pp. 407–417. ISSN: 1434-6001.

[17] Alain Boudard et al. "New potentialities of the Lige intranuclear cascade model for reactions induced by nucleons and light charged particles". In: *Phys.Rev.* C87.1 (2013), p. 014606.

[18] T. T. Boehlen et al. "Benchmarking nuclear models of FLUKA and GEANT4 for carbon ion therapy". In: *Physics in Medicine and Biology* 55.19 (2010), p. 5833.

[19] J. Dudouet et al. "Benchmarking geant4 nuclear models for hadron therapy with 95 MeV/nucleon carbon ions". In: *Physical Review C* 89 (2014), p. 054616.

[20] D. Kirkby W. Verkerke. *The RooFit Toolkit for Data Modeling.* URL: https://root.cern.ch/drupal/content/roofit.

[21] N. Olsson, E. Ramstrm, and B. Trostell. "Neutron elastic and inelastic scattering from beryllium, nitrogen and oxygen at En = 21.6 MeV". In: *Nuclear Physics A* 509.1 (1990), pp. 161 –177. ISSN: 0375-9474.

[22] M. De Napoli et al. "Carbon fragmentation measurements and validation of the Geant4 nuclear reaction models for hadrontherapy". In: *Physics in Medicine and Biology* 57.22 (2012), p. 7651.

[23] M. Kraemer et al. "Treatment planning for heavy-ion radiotherapy: physical beam model and dose optimization". In: *Physics in Medicine and Biology* 45.11 (2000), p. 3299.